Magnetic and optical properties of the InCrN system

P. A. Anderson,[a] R. J. Kinsey, and S. M. Durbin
Department of Electrical and Computer Engineering, The MacDiarmid Institute, University of Canterbury, Private Bag 4800, Christchurch, New Zealand

A. Markwitz and V. J. Kennedy
Institute of Geological and Nuclear Sciences, The MacDiarmid Institute, Lower Hutt, New Zealand

A. Asadov and W. Gao
Department of Chemical and Materials Engineering, University of Auckland, Private Bag 92006, Auckland, New Zealand

R. J. Reeves
Department of Physics and Astronomy, The MacDiarmid Institute, University of Canterbury, Private Bag 4800, Christchurch, New Zealand

(Received 26 January 2005; accepted 12 June 2005; published online 18 August 2005)

Room-temperature ferromagnetic $In_{1-x}Cr_xN$ films with x ranging from 0.0005 to 0.04 and antiferromagnetic CrN films have been grown by plasma-assisted molecular-beam epitaxy. Electron and x-ray-diffraction techniques could find no evidence for precipitates or phase segregation within the films. Ferromagnetism was observed in the $In_{1-x}Cr_xN$ layers over a wide range of Cr concentrations, with the magnitude of the ferromagnetism found to correlate with the background carrier concentration. Higher *n*-type carrier concentrations were found to lead enhanced ferromagnetism, with maximum saturation and remnant moments of 7 and 0.7 emu/cm^3, respectively. The addition of Cr to the InN matrix led to reduced photoluminescence intensity and a shift of the peak to higher energy. These observations along with a band-gap-like optical transmission feature at 0.7 eV suggest that CrN has an indirect gap of approximately 0.7 eV and a direct Γ-valley gap greater than 1.2 eV. © *2005 American Institute of Physics*.
[DOI: 10.1063/1.1993753]

I. INTRODUCTION

The area known as spintronics has attracted significant attention in recent years as various groups strive to develop an efficient spin alignment and injection technology.[1] One approach is to use a semiconductor with a fraction of the atoms substituted by a transition metal, known as a diluted magnetic semiconductor (DMS). The use of a DMS as a spin-polarizing layer avoids the obstacle of injecting spin-polarized electrons across a metal-semiconductor interface—a process which has hampered progress using conventional ferromagnets.[2] $Ga_{1-x}Mn_xAs$ and $In_{1-x}Mn_xAs$ were the first ferromagnetic DMS materials to be explored extensively, although their low Curie temperatures make them undesirable for practical applications.[3,4] A theoretical study by Dietl *et al.*[5] predicted higher Curie temperatures for a wide-band-gap semiconductors, and experimental studies confirmed room-temperature ferromagnetism in a number of materials including $Ga_{1-x}Mn_xN$, $Ga_{1-x}Cr_xN$, $Al_{1-x}Cr_xN$, $Zn_{1-x}Co_xO$, $Ti_{1-x}Co_xO_2$, and $Sn_{1-x}Co_xO_2$.[6–10]

Of these materials, the nitride semiconductors have the advantage of an existing and rapidly developing technology base, which to date has been driven by blue and UV optical device applications. Despite the important role of InN in this industry, and recent interest regarding the value of the band gap,[11,12] there have been only two reports on its use as a DMS host. Specifically, Chen *et al.* observed hysteresis at 1.7 K in an $In_{0.9}Mn_{0.1}N$ film.[13] A related study by the same group identified above room-temperature ferromagnetism in an $In_{0.98}Cr_{0.02}N$ film.[14]

The two binary end points of the InCrN alloy, diamagnetic InN and antiferromagnetic CrN,[15] are not well understood optically. The band gap of InN has been hotly debated, now appear that the majority of researchers in the field support a band gap near 0.7 eV.[11,12] Studies on the optical properties of CrN, however, have been sparse—with both metallic[16,17] and semiconducting[18,19] behaviors being reported from bulk and sputtered materials.

In this report we study the magnetic, microstructural, and optical properties of a series of $In_{1-x}Cr_xN$, InN, and CrN films grown by plasma-assisted molecular-beam epitaxy (PAMBE). The diffraction experiments find no evidence of multiple phases or precipitates within the layers. High Curie temperatures within the $In_{1-x}Cr_xN$ material system are confirmed and the dependence of the magnetic properties on Cr content and carrier concentration is explored. Photoluminescence and optical transmission measurements on InN, CrN, and $In_{1-x}Cr_xN$ support a band gap near 0.7 eV for InN and suggest that CrN has an indirect band gap, also around 0.7 eV.

II. EXPERIMENTAL PROCEDURE

A Perkin-Elmer PAMBE system with a low base pressure of 10^{-10} Torr was used for the growth of InN, CrN, and $In_{1-x}Cr_xN$ films. Active nitrogen was supplied with an Ox-

[a]Electronic mail: p.anderson@elec.canterbury.ac.nz

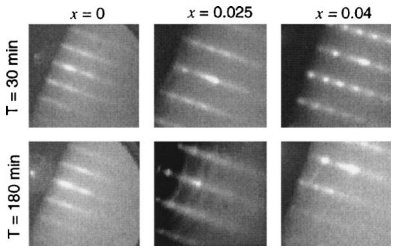

FIG. 1. RHEED images taken after 30 min and at the end of growth (180 min) for three $In_{1-x}Cr_xN$ films, grown under identical conditions except for the Cr content.

ford Applied Research HD25 rf plasma source operating at 1.25 SCCM (standard cubic centimeter per minute) and 250 W, and In, Ga, and Cr were supplied by effusion cells with fluxes of approximately 10^{14} cm^{-2} s^{-1}, as measured by a water-cooled quartz-crystal microbalance. (0001) sapphire substrates were used for all film growth experiments after nitriding for 15 min at 650 °C. For $In_{1-x}Cr_xN$ growth a 150-nm GaN buffer layer was deposited at 650 °C, followed by 150 nm of InN at 450 °C, and finally 700 nm of $In_{1-x}Cr_xN$ at 450 °C. CrN films were deposited directly on the nitrided sapphire and were 500 nm thick. Growth rates for InN, $In_{1-x}Cr_xN$, CrN, and GaN were ~250 nm/h. The growth was monitored *in situ* by 20-kV reflection high-energy electron diffraction (RHEED). The structural characterization included atomic force microscope (AFM), x-ray diffraction (XRD), and electron backscatter diffraction (EBSD). Magnetic measurements were made with a Quantum Design superconducting quantum interference device (SQUID) magnetometer and Hall-effect measurements utilized an EGK-2000 0.5-T system. The stoichiometry of the film was determined using a combination of Rutherford backscattering spectrometry (RBS), nuclear reaction analysis (NRA), and particle-induced x-ray emission (PIXE).[20] Optical characterization included near-infrared-absorption measurements with a custom-built system incorporating a tungsten lamp and lead sulphide detector, and photoluminescence was performed with an argon laser operating at 488 nm and either a germanium or indium antimonide detector.

III. RESULTS AND DISCUSSION

The $In_{1-x}Cr_xN$ films, having x ranging from 0.0005 to 0.04, each exhibited a total metal to nitrogen ratio of essentially unity as determined by ion-beam analysis. The elemental concentrations were obtained with three different ion-beam techniques. NRA was used to determine the total amount of nitrogen in the films, which in turn was used to verify the nitrogen content obtained from RBS. Furthermore, the chromium concentrations measured with PIXE confirmed the values obtained by RBS. Figure 1 shows the RHEED patterns for three films of varying Cr content after 30 and 180 min into growth. Increased Cr content was found to lead to progressively degraded crystal quality, as indicated by RHEED patterns which changed from streaky for $x<0.025$, to spotty with weak arcs visible in the case of $x=0.025$ and 0.04. This suggests that there is some *a*-plane rotation between crystal domains in these films, whereas the lower chromium concentration films have good alignment between the domains in the *a* plane. The film grown with $x=0.04$ partially delaminated from the GaN buffer layer, signaling the high level of stress present in the film. This observation is surprising as the lattice match between $In_{1-x}Cr_xN$ and GaN improves with increasing Cr content, assuming that chromium occupies the cation lattice site.

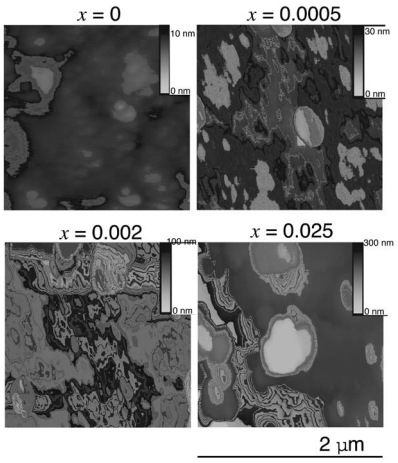

FIG. 2. AFM images of four $In_{1-x}Cr_xN$ films with varying chromium content.

AFM, EBSD, and XRD were used to search for any evidence of phase separation within the films. AFM revealed that the film surfaces contained plateaus exhibiting a hexagonal symmetry which covered the increasing proportions of the surface with higher film chromium content, as shown in Fig. 2. The film morphology quickly departs from the smooth appearance of InN with rms roughness <5 nm, to the highly plateaued surfaces of the higher Cr content films with rms roughness >50 nm. EBSD is a structurally sensitive technique which can map the crystal structure of the near-surface region. EBSD showed that the hexagonal plateaus had the same crystal structure and orientation as the rest of the film, suggesting that they are not precipitates but a product of the growth mode of the films. We have also observed this growth behavior in InN grown at low substrate temperatures.

Figure 3 shows the two-theta XRD curves for three high Cr content films. Only features expected from a *c*-axis-oriented wurtzite structure are observed. The weak indium metal peak at 33° originates from In on the backside of

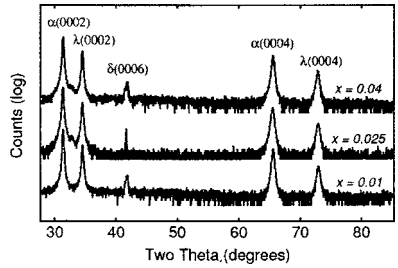

FIG. 3. Two-theta x-ray diffraction scans for $In_{1-x}Cr_xN$ films with $x=0.01$, 0.025, and 0.04; α denotes InN, λ denotes GaN, and δ denotes sapphire peaks. The curves are displaced from each other for clarity.

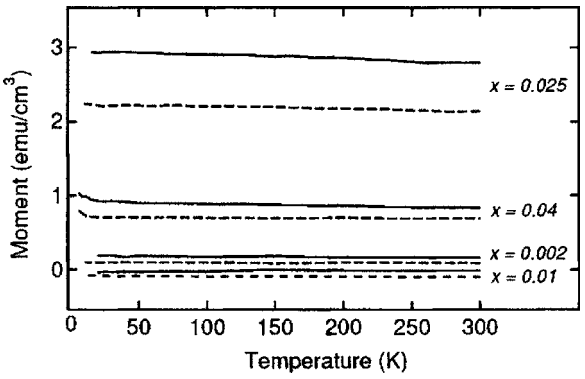

FIG. 4. Magnetization vs temperature measurements at 20 mT for $In_{1-x}Cr_xN$ films grown under identical conditions, except for the Cr content. The films were either demagnetized (dashed curves) or poled at 1 T (solid curves) before beginning the temperature sweep. The displacement between the two curves indicates the level of ferromagnetic component.

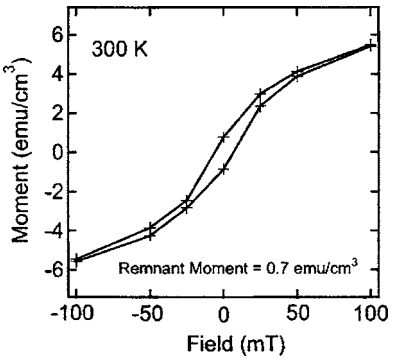

FIG. 5. Magnetization vs applied field measurement at 300 K for an $In_{0.975}Cr_{0.025}N$ film. The field was set at ±1 T in order to saturate the magnetization of the sample before beginning the magnetic-field sweeps.

the substrate, used to mount the sample. The $\alpha(0002)$ peak positions for $x=0.01$, 0.025, and 0.04 correspond to diffraction plane spacings of 2.9594, 2.9644, and 2.9610 Å, respectively. For $x>0.025$ the spacings indicate that the *c*-axis lattice constant is actually increasing with the addition of the much smaller Cr atoms, contrary to the expected dependence of Vegard's law. This is likely due to a significant amount of the Cr occupying interstitial sites. However, the diffraction spacing for the $x=0.04$ film is less than that of the $x=0.025$ film, suggesting that there are two competing processes. It seems likely that Cr is occupying both substitutional and interstitial sites with the different locations having competing effects on the measured lattice constant.

Temperature-dependent magnetization measurements taken at 20 mT after the samples have been demagnetized (dashed curves), and then again with the samples magnetized (solid curves) are shown in Fig. 4. The displacement between each pair of curves persists throughout the temperature range, indicating that ferromagnetism remains in all samples at 300 K. Further investigation of the $x=0.025$ and 0.04 samples by vibrating-sample magnetometer (VSM) revealed hysteresis persisting to 470 K; above this temperature, the signal-to-noise level in the system prevented further exploration. Interestingly all of the films show a little increase in the magnetic moment at low temperatures. This effect is common among DMS materials and arises from enhancements in the magnetic susceptibility of paramagnetic ions within the film (somewhat evident in the $x=0.025$ sample). The absence of a strong paramagnetic component indicates that ordered magnetic states are dominating the response. The maximum magnetic moment is observed in the $x=0.025$ sample, with the lower Cr concentrations displaying a very weak ferromagnetism.

Figure 5 shows the room-temperature hysteresis loop for the film with $x=0.025$. The measured saturation moment of 7 emu/cm^3 corresponds to a moment of 1 Bohr magneton per Cr atom, and the remnant moment of 0.7 emu/cm^3 and coercive field of 7 mT are both comparable with other nitride-based DMS at room temperature, including the $In_{0.98}Cr_{0.02}N$ examined by Chen *et al.*[14,21]

Electrical measurements on the films revealed an increase in the *n*-type carrier concentration from $\sim 10^{19}$ cm^{-3} for undoped InN to $(0.8–9)\times 10^{20}$ cm^{-3} for the Cr-doped films. Transition metals typically occupy the cation lattice site and act as an effective-mass acceptor in III-V semiconductors.[21] However, 3*d* shell energy estimates by Dietl and Ohno using the Vonsovskii model suggest that Cr may act as a donor in InN.[22] Alternatively, the increased carrier concentrations may be related to interstitial Cr. This hypothesis is supported by XRD measurements which show that a significant amount of the Cr is incorporating interstitially. Additionally, the *n*-type carrier concentration is found to be highest in the films with the largest *c*-axis lattice constant and hence greatest number of interstitial chromium atoms, again supporting interstitial Cr acting as a donor. Consistent with the degradation of the RHEED patterns, the Hall mobility decreased with increasing Cr content, from 250 cm^2/V s for $x=0$, to 35 cm^2/V s for $x=0.04$. Figure 6 shows the moment between the magnetized and demagnetized curves of Fig. 4 as a function of carrier concentration. A clear correlation between *n*-type carrier concentration and magnetic moment is observed. This is a surprising result as most theoretical treatments of III-V DMS predict that holes are required to mediate the exchange interaction.[5] The enhancement in ferromagnetism is similar to the observations by Story *et al.* who found a change in magnetic ordering in PbSnMnTe at comparable *p*-type carrier concentrations.[23] Comparable changes in the magnetic state of InMnAs have been shown to occur at the lower *p*-type carrier concentrations around 10^{19} cm^{-3}.[24]

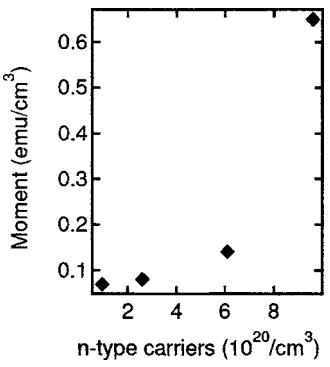

FIG. 6. Ferromagnetic component of Fig. 4 at 300 K vs the corresponding carrier concentrations of the films.

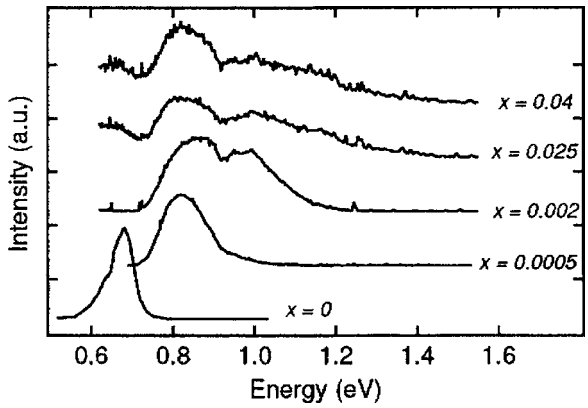

FIG. 7. Photoluminescence signals obtained from $In_{1-x}Cr_xN$ films with varying values of x. The curves are displaced from each other for clarity.

The binary end points of the alloy—CrN and InN—were studied along with the $In_{1-x}Cr_xN$ films in order to gain an understanding of the optical properties of the material system. CrN films were grown on (0001) sapphire at substrate temperatures in the range of 250–650 °C with 650 °C found to give the lowest electron concentration and highest mobilities of 9×10^{18} cm^{-3} and 70 cm^2/V s, respectively. The films were identified as (111)-oriented rocksalt-phase CrN by XRD. SQUID measurements confirmed that the material was antiferromagnetic with a Néel temperature near 280 K. Details of InN film growth and properties are described elsewhere.[25]

InN luminesces brightly near 0.7 eV, which is now generally believed to reflect a band-gap energy of comparable value. The addition of Cr to the InN matrix was found to reduce the photoluminescence (PL) intensity and lead to multiple features at higher energies, as shown in Fig. 7. Attempts were made to obtain a PL signal from CrN but nothing above background noise was observed.

With PL failing to reveal any meaningful information on the band structure of CrN, temperature-dependent resistivity and optical transmission and reflection measurements were performed as an alternative approach. Figure 8 shows the temperature-dependent resistivity of a CrN film grown at 650 °C. The resistivity increases slowly with decreasing temperature, suggesting some semiconductorlike carrier freeze-out, although there appears to be a large degenerate background concentration which is not unreasonable considering the measured carrier concentrations. A step in the resistivity

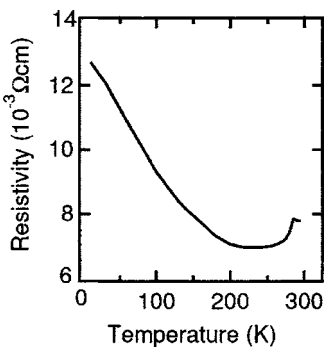

FIG. 8. The temperature-dependent resistivity of a CrN film.

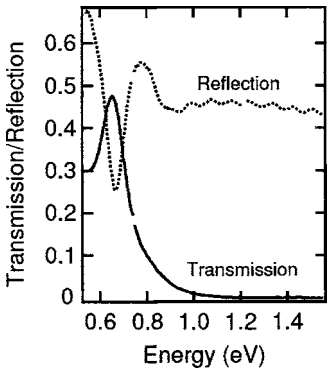

FIG. 9. The transmission and reflection of a CrN film showing a band-edge-like feature near 0.7 eV.

is observed at the Néel temperature, confirming earlier reports on bulk samples which identified a change in the electrical properties of the material at the Néel temperature.[17,26]

Optical transmission and reflection spectra of CrN are shown in Fig. 9. These results confirm the observations by Gall *et al.* who saw a similar band-gap-like feature near 0.7 eV.[18] The reduction in transmission from 0.48 to less than 0.01, coupled with the temperature-dependent resistivity measurements, points to CrN being semiconducting with a band gap close to 0.7 eV. The lack of PL from the material suggests that the fundamental band gap is indirect. A Γ-valley gap of >0.7 eV with an indirect gap near 0.7 eV can be used to explain the PL results and the infrared-absorption data. Upon addition of Cr to the InN matrix, the direct gamma valley gap increases, which explains the appearance of the higher-energy components in Fig. 7. Further, momentum conservation results in a rapid dampening of radiative recombination and hence PL. However, creation of electron-hole pairs via absorption is not inhibited to the same extent by the momentum constraint, and hence CrN still exhibits strong transmission and reflection features near 0.7 eV.

IV. CONCLUSIONS

In conclusion, $In_{1-x}Cr_xN$ films with x ranging from 0.0005 to 0.04, as well as the binary end points InN and CrN, have been grown on sapphire using a PAMBE technique. Cr doping was found to lead to a high concentration of *n*-type carriers, and a degradation of the crystal quality as observed by RHEED. Magnetic characterization revealed the room-temperature ferromagnetism in all InCrN films with the magnitude of the ferromagnetic signal increasing with *n*-type carrier concentration. The highest saturation and remnant moment achieved were 7 and 0.7 emu/cm^3, respectively, for a film with $x=0.025$, and an electron concentration of 9×10^{20} cm^{-3}. Increasing the Cr concentration in $In_{1-x}Cr_xN$ led to a shift in PL to higher energy and a reduction in PL intensity. Transmission and reflection results showed a band-gap-like feature near 0.7 eV within CrN films and no distinguishable PL, consistent with an indirect gap near 0.7 eV for CrN. The magnetic properties of $In_{1-x}Cr_xN$ compare well with other nitride-based DMS and the possibility of electron-mediated ferromagnetism makes these unintentionally *n*-type materials far more promising candidates for future devices.

ACKNOWLEDGMENTS

The authors would like to thank Dr. Dennis Leung from the Department of Materials Science and Metallurgy, University of Cambridge for VSM, Dr. Milo Kral from the Department of Mechanical Engineering, University of Canterbury for EBSD, Chito Kendrick, Lyndon Williams, and Annette Koo for experimental assistance, and Gary Turner for engineering support. This work is funded in part by the MacDiarmid Institute for Advanced Materials and Nanotechnology, and the University of Canterbury.

[1]S. A. Wolf, D. D. Awschalom, R. A. Buhrman, J. M. Daughton, S. von Molnar, M. L. Roukes, A. Y. Chtchelkanova, and D. M. Tregger, Science **294**, 1488 (2001).
[2]V. F. Motsnyi, J. D. Boek, J. Das, W. V. Roy, and G. Borghs, Appl. Phys. Lett. **81**, 265 (2002).
[3]H. Ohno, A. Shen, F. Matsukura, A. Oiwa, A. Endo, S. Katsumoto, and Y. Lye, Appl. Phys. Lett. **69**, 363 (1996).
[4]H. Ohno, H. Munekata, T. Penney, S. von Molnar, and L. L. Chan, Phys. Rev. Lett. **68**, 2664 (1993).
[5]T. Dietl, H. Ohno, and F. Matsukura, Phys. Rev. B **63**, 195205 (2001).
[6]D. Kumar, J. Antifakos, M. G. Blamire, and Z. H. Barber, J. Appl. Phys. **84**, 5004 (2004).
[7]S. B. Oagle *et al.*, Phys. Rev. Lett. **91**, 077205 (2003).
[8]W. K. Park, R. J. Ortega-Hertogs, and J. S. Moodera, J. Appl. Phys. **91**, 8093 (2002).
[9]K. H. Kim, K. J. Lee, D. J. Kim, H. J. Kim, and Y. E. Ihm, Appl. Phys. Lett. **82**, 4755 (2003).
[10]A. F. Hebard, R. P. Rairigh, J. G. Kelly, S. J. Pearton, C. R. Abernathy, S. N. G. Chu, and R. G. Wilson, J. Phys. D **37**, 511 (2004).
[11]J. Wu *et al.*, Appl. Phys. Lett. **80**, 21 (2002).
[12]V. Y. Davydov *et al.*, Phys. Status Solidi B **229**, R1 (2001).
[13]P. P. Chen, H. Makino, and T. Yao, Solid State Commun. **130**, 25 (2004).
[14]P. P. Chen, H. Makino, and T. Yao, J. Cryst. Growth **269**, 66 (2004).
[15]L. M. Corliss, N. Elliot, and J. M. Hastings, Phys. Rev. **117**, 929 (1960).
[16]A. Filipetti, W. E. Pickett, and B. M. Klein, Phys. Rev. B **59**, 7043 (1999).
[17]J. D. Browne, P. R. Liddell, R. Street, and T. Mills, Phys. Status Solidi **1**, 715 (1970).
[18]D. Gall, C.-S. Shin, R. T. Haasch, I. Petrov, and J. E. Greene, J. Appl. Phys. **91**, 5882 (2002).
[19]P. S. Herle, M. S. Hegde, N. Y. Vasathacharya, and S. Philip, J. Solid State Chem. **134**, 120 (1997).
[20]J. R. Bird and J. S. Williams, *Ion Beams for Materials Analysis* (Academic, Bowen Hills, Australia, 1989).
[21]S. J. Pearton *et al.*, J. Appl. Phys. **93**, 1 (2003).
[22]T. Dietl and H. Ohno, MRS Bull. **28**, 714 (2003).
[23]T. Story, R. R. Gatazka, R. B. Frankel, and P. A. Wolff, Phys. Rev. Lett. **56**, 777 (1986).
[24]S. Koshihara, A. Oiwa, M. Hirasawa, S. Katsumoto, Y. Iye, C. Urano, and H. Takagi, Phys. Rev. Lett. **78**, 4617 (1997).
[25]R. J. Kinsey, P. A. Anderson, C. E. Kendrick, R. J. Reeves, and S. M. Durbin, J. Cryst. Growth **269**, 166 (2004).
[26]Y. Tsuchiya, K. Kosuge, Y. Ikeda, T. Shigematsu, S. Yamaguchi, and N. Nakayama, Mater. Trans., JIM **37**, 121 (1996).